Dielectric Properties of Healthy Ex Vivo Ovine Lung Tissue at Microwave Frequencies

Klementina Vidjak, Laura Farina, *Member, IEEE*, Giuseppe Ruvio, *Senior Member, IEEE*, Martin O'Halloran, *Member, IEEE*, and Marta Cavagnaro, *Senior Member, IEEE*

***Abstract*—Knowledge of dielectric properties of lung tissue is fundamental for the improvement of lung disease diagnostics and therapeutic solutions [e.g., microwave imaging (MWI) and microwave thermal ablation (MWA) treatment]. Although lung disease rates are increasing, lung tissue remains one of the least characterized tissues due to its heterogeneity, variability in air content, and handling difficulties. In this work, the dielectric properties of ex vivo ovine lung tissue samples were measured in the frequency range 500 MHz–8 GHz, together with measurements of sample density (air content). Different Cole–Cole models were applied to the measured dielectric properties values. The best fitting model was chosen, and results were compared with available literature. Furthermore, the dielectric property measurements were correlated with the air content of the samples. Updated Cole–Cole models for the lung tissue of different densities are provided in the 500 MHz–8 GHz range. The existence of air content threshold in lung is shown. Below this limit, the properties begin to change drastically with the change in density.**

***Index Terms*—Cole–Cole model fitting, dielectric spectroscopy, lung tissue air content, lung tissue dielectric properties, open-ended coaxial probe.**

I. Introduction

KNOWLEDGE of tissue dielectric properties is paramount in various electromagnetic-based medical applications, such as diagnostics, therapy, dosimetry, and monitoring. A diagnostic and monitoring technique relying on dielectric properties knowledge is microwave imaging (MWI) [1]. MWI determines the position of healthy and malignant tissue based on contrast in dielectric properties. Examples of its use from the literature are in the liver [2], and lately, in lung tissue [3]. A therapeutic technique that benefits from an accurate knowledge of the dielectric properties is microwave thermal ablation (MWA) [2], [4], [5].

While tissues, such as liver [5], [6], [7], heart [6], muscle [5], [6], [8], and breast tissue [9], are well characterized, lung tissue remains insufficiently studied in the microwave range due to handling difficulties and tissue heterogeneity [6].

Nevertheless, the number of lung diseases diagnosed yearly is continuously rising, the incidence of lung cancer is second only to breast, and it is the first cause of cancer death worldwide [10]. Alongside the recent focus on microwave-based clinical solutions [11], [12], the investigation of lung dielectric properties represents a need and should be carefully addressed.

To date, the usual reference for the dielectric properties of biological tissues is the IT'IS database [13], based on [5], where the properties and associated densities of ex vivo lung are reported. In particular, the dielectric properties are based on [5], where lung tissue was categorized in two classes, with respect to the inflation level: fully inflated and deflated lung [5]. However, in [5], no information is provided on the number of inflated and deflated samples used in the measurements neither on the technique used to achieve inflated and deflated states or the associated density of the tissue. Accordingly, tissue density information in [13] is taken from [14]. Besides [5], only other three studies performed lung dielectric characterization in the microwave range, all of them in 2019 [6], [15], [16]. Fornes-Leal et al. [6] measured in vivo porcine lungs in the frequency range 0.5–26.5 GHz. Bonello et al. [15] investigated the changes of ex vivo ovine lung dielectric properties with temperature in the frequency range 0.5–8 GHz. Finally, Sebek et al. [16] investigated broadband lung dielectric properties over the ablative temperature range in the frequency range 0.5–6 GHz. These studies gave interpolation models of the measured data. They all give dielectric properties of lung tissue higher with respect to the four-pole Cole–Cole model for inflated lung reported in the IT'IS database [13], but lower than the deflated lung dielectric properties from the Gabriel and Gabriel [5] study. Attempts to model dielectric properties of lung as a function of air content have been made by Nopp et al. [17] in the 5–100 kHz range and by Etoz and Brace [18] in the 1–15 GHz range [18]. The latter research combines coupled dielectric relaxation models (Cole–Cole and Debye) and mixture terms (Maxwell–Fricke and Maxwell) to model the dielectric properties of ex vivo

Manuscript received 1 October 2022; revised 5 January 2023; accepted 26 February 2023. Date of publication 8 March 2023; date of current version 1 June 2023. This research was funded by Government of Ireland, Disruptive Technology Innovation Fund (DTIF), grant number DT2020189. *(Corresponding author: Klementina Vidjak.)*

Klementina Vidjak and Marta Cavagnaro are with the Department of Information Engineering, Electronics and Telecommunications, Sapienza University of Rome, 00184 Rome, Italy (e-mail: klementina.vidjak@uniroma1.it; marta.cavagnaro@uniroma1.it).

Laura Farina and Giuseppe Ruvio are with Endowave Ltd., H91 DCH9 Galway, Ireland.

Martin O'Halloran is with the University of Galway, H91 TK33 Galway, Ireland.

Color versions of one or more figures in this article are available at https://doi.org/10.1109/TDEI.2023.3253812.

Digital Object Identifier 10.1109/TDEI.2023.3253812

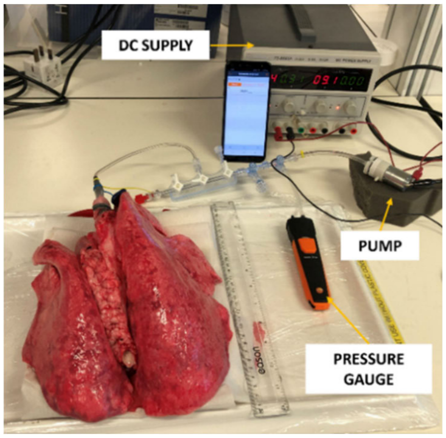

Fig. 1. Inflation setup for achieving fully inflated lung.

bovine liver and lung tissue. Still, the obtained models have a large deviation from measured data. Accordingly, a more extensive study of lung tissue dielectric properties is required, especially in the context of its inflation level.

In this work, $N_s = 79$ samples were extracted from $N_l = 6$ pairs of ex vivo ovine lungs. In order to understand the influence of air volume inside the lung on the measured dielectric properties, some lung samples were inflated prior to measurements using a vacuum pump. During the experiment, both density and dielectric properties in the frequency range 500 MHz–8 GHz were measured. Afterward, the Cole–Cole model [19] was used to fit the measured data. Additionally, an attempt to correlate the dielectric properties to the density was made.

II. Methods

A. Sample Preparation

Lung tissue was extracted from ex vivo ovine lung pairs obtained from a local abattoir. Lungs were requested intact, still connected with the heart and with the pleura to minimize tissue dehydration, blood loss, and air leakages during the inflation process. Samples were processed within 2 h after lung excision to minimize tissue dehydration and deterioration [20].

In total, 79 cubic-shaped samples were cut from six pairs of lungs; five pairs of lungs were inflated prior to sample extraction and one pair of lungs was used in the untreated, deflated state.

The inflation process was performed feeding air through the trachea for approximately 2 h at a pressure of about 29 mbar. This pressure level ensures the tissue recovery from the atelectasis occurring after the organ removal from the body [21]. The inflation process was validated through histology: no changes in the cellular structure nor disruption of the tissue architecture was observed. The inflation setup included the following apparatus (see Fig. 1): mini vacuum pump, dc power supply (12 V), Testo 510i pressure gauge, and tubes for air supply. During the procedure, the lung was covered with polyethylene plastic film to minimize dehydration and therefore the change in properties. However, the influence on the measured dielectric properties of possible tissue desiccation cannot be ruled out.

Three to four cubic-shaped samples were randomly cut from the lungs, by avoiding big airways that can impair the dielectric properties and density measurements.

B. Density Measurements

Density was calculated for each lung cubic sample. To determine the density of cubic-shaped samples, the general formula was used

$$\rho = \frac{m}{V} \tag{1}$$

where V is the volume of the sample and m is its mass.

The volume was determined by measuring the height (h), length (l), and width (w) of the cube with a ruler. The mass of each cube was measured using a precision KERN EMB 600-2 scale. The calculated density was expressed in kg/m^3 [22].

The measurement uncertainty arises from both volume and mass measurements. In the case of the volume, the uncertainty arises from the ruler's resolution of 0.05 cm and from deviations of the samples from being actual cubes.

The ruler accuracy shows a rectangular distribution; therefore, it must be divided by $\sqrt{3}$ to calculate the combined uncertainty of the volume. On the other hand, the uncertainty contribution associated with the shape of the sample was assessed measuring the cube edges three times and assigning to each edge the average among the measurements; additionally, only those cubes in which the maximum difference in the three edge measurements was 0.1 cm were retained. The corresponding uncertainty is given by the standard deviation of the mean (SDM). Thus, the volume combined uncertainty is given by the following equation [23]:

$$\frac{\delta V}{V} = \sqrt{\begin{array}{l}\left(\frac{\delta l_1}{l}\right)^2 + \left(\frac{\delta l_2}{l} * \frac{1}{\sqrt{3}}\right)^2 + \left(\frac{\delta w_1}{w}\right)^2 + \cdots \\ \left(\frac{\delta w_2}{w} * \frac{1}{\sqrt{3}}\right)^2 + \left(\frac{\delta h_1}{h}\right)^2 + \left(\frac{\delta h_2}{h} * \frac{1}{\sqrt{3}}\right)^2\end{array}} \tag{2}$$

where δl_1, δw_1, and δh_1 are calculated as an SDM based on the three repetitive measurements, and δl_2, δw_2, and $\delta h_2 = 0.05$ cm.

In the case of mass measurement, the scale introduces two uncertainties, readout ($u_{\text{read}} = 0.001$ g), and linearity ($u_{\text{read}} = \pm 0.005$ g). Both uncertainty components show a rectangular distribution. Therefore, the combined uncertainty of mass can be expressed as [23]

$$\frac{\delta m}{m} = \sqrt{\left(\frac{u_{\text{read.}}}{m} * \frac{1}{\sqrt{3}}\right)^2 + \left(\frac{u_{\text{lin.}}}{m} * \frac{1}{\sqrt{3}}\right)^2}. \tag{3}$$

The total uncertainty for density is therefore calculated through the following equation [23]:

$$\frac{\delta \rho}{\rho} = \sqrt{\left(\frac{\delta V}{V}\right)^2 + \left(\frac{\delta m}{m}\right)^2}. \tag{4}$$

After each density measurement, the lung cubes were sealed in plastic containers to minimize tissue dehydration and deterioration before the dielectric property measurements [20].

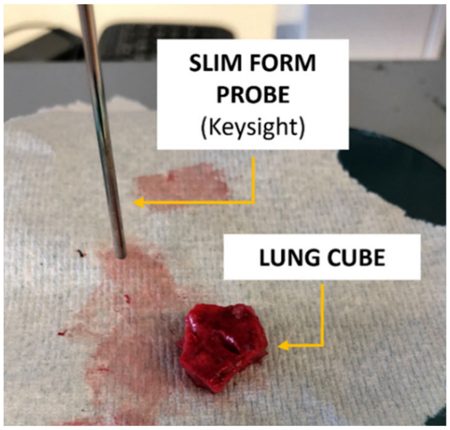

Fig. 2. Example of dielectric properties measurement on a lung cube.

C. Dielectric Properties Measurements

Dielectric properties of the samples were measured using the open-ended coaxial probe technique (see Fig. 2) [24]. The dielectric measurements were performed right after the measurement of tissue density. In this experiment, the Keysight 85070E slim form probe was used with the Keysight E5063A vector network analyzer (VNA), equipped with the Keysight software for dielectric properties evaluation (N1500A). The operating frequency ranges of the slim form probe and the used VNA devices are 0.5–50 GHz and 100 kHz–8.5 GHz, respectively. Therefore, the measurements were conducted in the frequency range 0.5–8 GHz with a 50 MHz step resulting in 151 linearly spaced frequency points. Calibration was performed using open circuit, short circuit, and distilled water. Temperature of distilled water was measured during each calibration procedure and was always between 23.5 °C and 24.5 °C. Calibration verification was performed by measuring the dielectric properties of 0.1 M NaCl solution [25], [26]. During the experiments, the cubic samples were placed on a lift with a screw, which was used to put the cubes in contact with the open end of the dielectric probe, without inducing movements in the low-noise cable connecting the probe with the VNA. The samples' temperature was measured prior to each dielectric measurement using two fiber optic probes (Neoptix Inc., Québec, QC, Canada). The samples' temperature was 24.7 °C ±1.3 °C.

A small incision was made in the sample to allow the tip of the probe to be embedded in the tissue and to minimize the effect of dehydration of the surfaces exposed to the measurements. If any blood leakages were present in the incision spot, they were dried gently using a paper towel. The pressure at the coaxial probe–tissue interface was adjusted with the use of the lift, while the appropriate pressure applied was identified based on preliminary dielectric readings and visual inspection. To increase result confidence, measurements were repeated five times in the same spot of the cube, for a total of 395 measurement acquisitions. In between each measurement, the probe was taken out and cleaned with an alcohol wipe to prevent result impairment due to blood or tissue residue from the previous take.

For these measurements, the measurement uncertainty arises from two factors.

Accuracy, which is the percentage deviation between measured and literature data on a well-characterized liquid, which was calculated using 0.1 M NaCl solution (calibration verification) [25],

Repeatability, or percentage SDM, which represents the random errors and that was obtained from the five repetitive measurements in the same spot of the cube.

For the calculation of the uncertainty of the density measurements, the combined uncertainty is calculated as the square root of the arithmetic sum of the square of the best estimation of each contribution [23].

D. Cole–Cole Model Fitting

The complex permittivity of biological materials in a broad frequency range can be expressed with a Cole–Cole model with four poles and a static conductivity term [19]. This model was used to represent the behavior of tissues' properties from 10 Hz to 100 GHz [5]

$$\hat{\varepsilon}(\omega) = \varepsilon_\infty + \sum_{i=1}^{4} \frac{\Delta_i}{1 + (j\omega\tau_i)^{1-\alpha_i}} + \frac{\sigma_s}{j\omega\varepsilon_0} \quad (5)$$

where ε_∞ is the permittivity at infinite frequency, Δ_i is the change of permittivity of the ith dispersion, τ_i is the time constant of the ith dispersion, α_i is an empirical parameter for broadening the dispersion, σ_s is the static conductivity term, ω is the angular frequency, and ε_0 is the permittivity of vacuum.

In this experiment, the measured data were fit to models with decreasing number of poles, i.e., from four to one, using the weighted least squares algorithm (W-LSM) [27]. This algorithm uses a complex weight factor to control and improve the fitting. Allowable error $\dot{e}_I$ is calculated as follows [27]:

$$\dot{e}_I \approx \left\{\hat{\varepsilon}(\omega_i)\right\}^\xi \quad (6)$$

where $\hat{\varepsilon}(\omega_i)$ is the measured permittivity at frequencyω_i. The power factor ξ is in this case equal to 0.75, putting more weight on the lower frequency data. The nonlinear least square method (LSM) is used with the Newton iterative method to minimize the total weighted and the squared error as

$$E^2 = \sum_{i=1}^{N_f} \left[\frac{\{c_r(\omega_i) - d_r(\omega_i)\}^2}{\{e_r(\omega_i)\}^2} + \frac{\{c_i(\omega_i) - d_i(\omega_i)\}^2}{\{e_i(\omega_i)\}^2} \right] \quad (7)$$

where $c_{r,i}(\omega_i)$ is either real or imaginary part of the calculated permittivity (obtained through fitting), $d_{r,i}(\omega_i)$ is either real or imaginary part of the measured permittivity, and $e_{r,i}(\omega_i)$ is either real or imaginary part of the allowable error ($\dot{e}_I$).

The overall fitting error in the real and imaginary part of complex permittivity is calculated using the following formula [27]:

$$\text{Error}_{\varepsilon'_{\text{avg}}, \varepsilon''_{\text{avg}}} = \sum_{i=1}^{N} \frac{\left| \frac{c_{r,i}(\omega_i) - d_{r,i}(\omega_i)}{d_{r,i}(\omega_i)} \right| \times 100}{N} \quad (8)$$

where N is the number of frequency acquisition points.

TABLE I
BEHAVIOR TREND OF COLE–COLE MODEL PARAMETERS WITH RESPECT TO THE TISSUE INFLATION LEVEL/DENSITY

Tissue type	ε_∞	Δ_1	$\tau_1[ps]$	α_1	Δ_2	$\tau_2[ns]$	α_2	σ_s	Δ_3	$\tau_3[\mu s]$	α_3	Δ_4	$\tau_4[ms]$	α_4
Deflated lung	4	45	7.958	0.1	1000	159.155	0.1	0.2	5e5	159.155	0.2	1e7	15.915	0
Inflated lung	2.5	18	7.958	0.1	500	63.662	0.1	0.03	2.5e5	159.155	0.2	4e7	7.958	0
Parameter behaviour	⬇	⬇	=	=	⬇	⬇	=	⬇	⬇	=	=	⬆	⬇	=

1) Choosing the Boundary Conditions of the Fitting Model: The success of W-LSM algorithm greatly depends on the provided bounds for the different parameters of the model. Therefore, choosing the appropriate limits is the biggest challenge. Appropriate boundary values have to contain the optimal solution but have to be not too large for the sake of computational time.

When implementing the algorithm in MATLAB, the initial values of the Cole–Cole model parameters were set randomly within the limit values. The latter were determined based on the observations of the parameter values obtained in the original four-pole Cole–Cole fitting from Gabriel and Gabriel [5]. Table I reports the model parameters for the two extreme cases of deflated and inflated lung as provided in [5]. In [13], the corresponding reference densities are reported as 1050 and 394 kg/m^3, respectively. Based on the first two rows, the third row of Table I indicates whether the fitting parameter values are increasing (arrow facing upward), decreasing (arrow facing downward), or are unchanged (equality sign) with respect to the level of inflation. On the other hand, in the present study, there were cubes with density lower than the inflated reference, so that it was assumed that the fitting algorithm boundaries must be expanded beyond the values of the parameters given in the second row of Table I. Therefore, the lower boundaries of the same parameters were set lower than the inflated reference. The values of ε_∞, Δ_1, Δ_2, τ_2, Δ_3, τ_4, and σ_s decrease with the increase of the level of inflation. The value of Δ_4 increases with the increase of the level of inflation, and the parameters α_1–α_4, τ_1, and τ_3 remain the same regardless of the tissue inflation level. Based on this observation and on the density range of the experimental cubes, the upper boundaries for ε_∞, Δ_1, Δ_2, τ_2, Δ_3, τ_4, and σ_s were set to those of deflated lung since no cube had a density larger than the deflated reference. The lower boundaries of the same parameters were set lower than the inflated reference. It should be noted that to achieve a reasonable computing time, both lower and upper limits were augmented based on a trial-and-error procedure after a few fitting tests were performed.

2) Two Step Fitting Procedure: The fitting of the measured dielectric properties to the Cole–Cole model was performed twice under two different conditions. First, the fitting was performed for all fitting parameters within sufficiently wide boundaries. Afterward, the parameter converging to the same value for over 80% of the lung cubes during the first fitting run was fixed for the second fitting attempt. In the second fitting, the algorithm tries to find the appropriate values for the remaining unfixed parameters to minimize the fitting error across the frequency range.

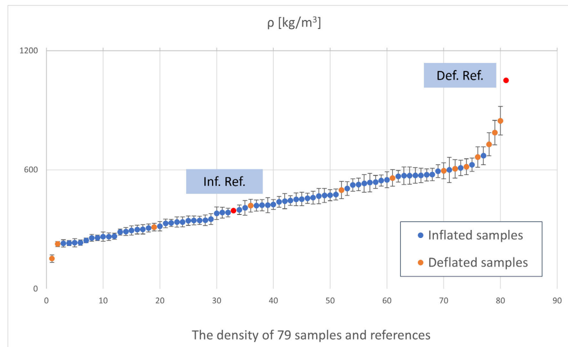

Fig. 3. Densities of all cubes with their measurement uncertainty aligned in an increasing order.

III. RESULTS

A. Experimental Results

Fig. 3 shows the density of the 79 samples together with the reference density for deflated and inflated lung (red points and a label) [13]. The deflated samples are presented with orange and inflated samples are presented with blue points. It must be underlined here that in this article, deflated lung stands for the lung as obtained from the abattoir, with no manipulation. All cubic samples satisfied the minimum thickness of 5 mm required for the measurements with the open-ended coaxial probe technique [28]. The smallest cubic sample had the volume of $7.84 \cdot 10^{-7}$ m^3, while the largest had the volume of $6.47 \cdot 10^{-6}$ m^3. Although 86% of the cubes were in an inflated state, their densities vary a lot, with the lowest measured density being 153 kg/m^3 and the highest 847 kg/m^3. The measurement uncertainty of density calculated with (3) is below 10% for all samples. When reference densities for inflated and deflated lung are compared to the results of this study, it can be observed that the inflated reference is aligned with the inflated cubes, while the deflated reference condition appears not achieved in this study. The results in Fig. 3 clearly show the high variability in density of lung tissue.

Fig. 4 shows the measured dielectric properties of the lung cubes over the frequency range 500 MHz–8 GHz. The blue curves represent the inflated, and the red curves represented the deflated samples.

Since the Keysight slim form probe manual states that the measurement accuracy using this type of probe is below 5%, the measurements that did not satisfy this criterion were

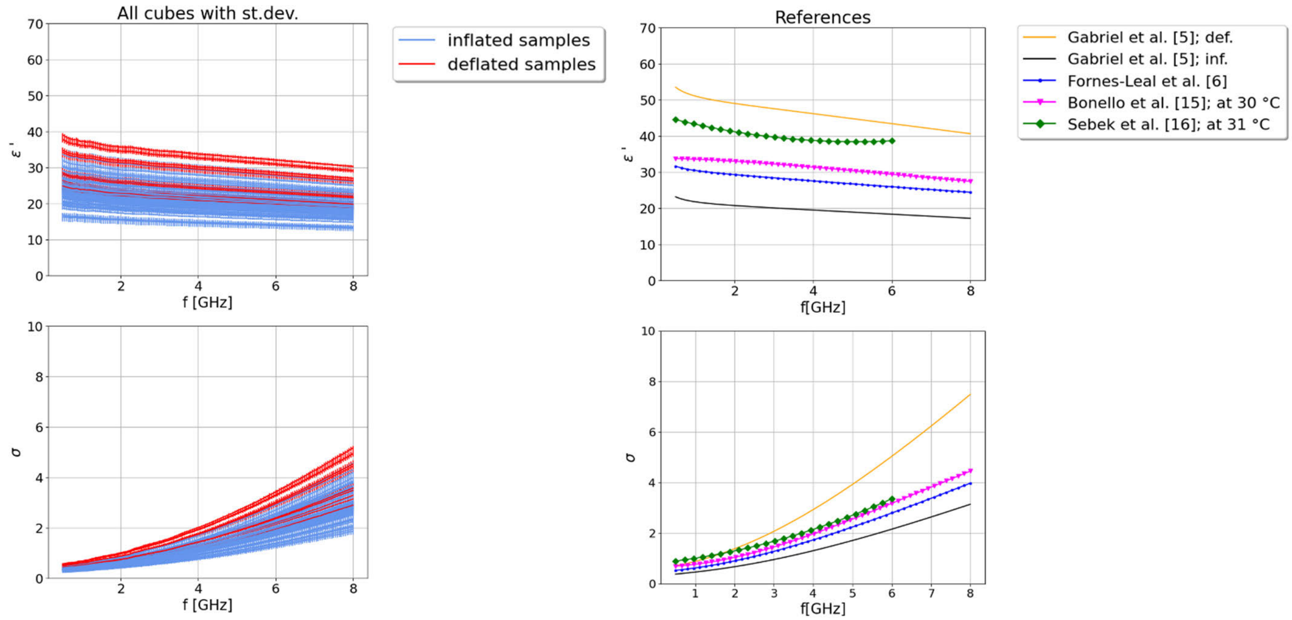

(a) (b)

Fig. 4. (a) Dielectric properties of all measured lung cubes with their uncertainty. (b) All lung dielectric properties references.

singled out, even though the combined uncertainty of all the samples was always below 10% for both permittivity and conductivity [28].

In particular, the uncertainty of permittivity is below 5% for 87% (69 cubes) of the samples, while the uncertainty of conductivity is below 5% for 77% (61 cubes) of the samples.

Accordingly, the dielectric properties of 61 ex vivo ovine lung cubes are plotted in Fig. 4(a) as the average value over the five repetitions with the measurement uncertainty. Fig. 4(b) shows the literature data. High variability is observed in the dielectric data in alignment with the variability observed in the density results as well as in the literature data. In particular, from Fig. 4(b), looking at the curves representing the data from [5], it can be derived that on average, the relative permittivity differs of 80.93% and the conductivity of 74.47% between inflated and deflated states. Similarly, data from the other published papers, even though all of them claim that measurements were performed without manipulation of the lung, in average differ up to 57.77% in relative permittivity and 37.62% in conductivity from the deflated lung reported in [5], respectively. Comparing with results in Fig. 4(a), it can be derived that the variability depends on the actual air content of the lung tissue.

B. Data Analysis

In this work, measurements were taken in the frequency band 500 MHz–8 GHz. Accordingly, in the search of the Cole–Cole fitting model, a number of poles smaller than four [5] could be foreseen. To determine the optimal number of poles, the data were fitted to models with decreasing number of poles, i.e., from four to one. The measured data were unsuccessfully fitted to four- and one-pole Cole–Cole models. Fitting the data to the three- and two-pole models resulted in very low fitting errors.

TABLE II

STARTING BOUNDARIES USED FOR THE THREE-POLE COLE–COLE MODEL FITTING AND THE FIXED PARAMETER VALUES FOR THE SECO FITTING

Boundary type	ε_∞	Δ_1	$\tau_1[ps]$	Δ_2	$\tau_2[ns]$	Δ_3	$\tau_3[\mu s]$	σ_s
Lower	1	10	7.5	200	20	2.5e5	150	0.001
Upper	7	45	8.5	1e3	160	5e5	196	0.2
Fixed values	/	/	7.5	600	160	3.75e5	195	0.001

1) Three-Pole Cole–Cole Model Fitting: For the three-pole Cole–Cole model, the data for each cube were fitted to (7) using three poles. The values of α_1–α_3 were fixed, since in the initial fitting attempts, they were always converging to the already given values (see Table I [5]). The remaining parameter values ε_∞, Δ_1, τ_1, Δ_2, τ_2, Δ_3, τ_3, and σ_s were calculated by the algorithm within the limits given in the first two rows of Table II.

The limits were determined as described in Section II-D1, in the effort of identifying the best tradeoff between computational time and solution inclusion. After the first fitting attempt, the values of τ_1, Δ_2, τ_2, Δ_3, τ_3, and σ_s, converged toward the same value for each respective parameter, as reported in the third row of Table II. Therefore, the fitting was performed once again to identify the remaining values ε_∞ and Δ_1.

Fig. 5 shows the resulting values calculated for ε_∞ and Δ_1.

The achieved fitting error in the real part is below 2% for each cube, while in the imaginary part, the error is always lower than 12% and lower than 5% for most of the cases.

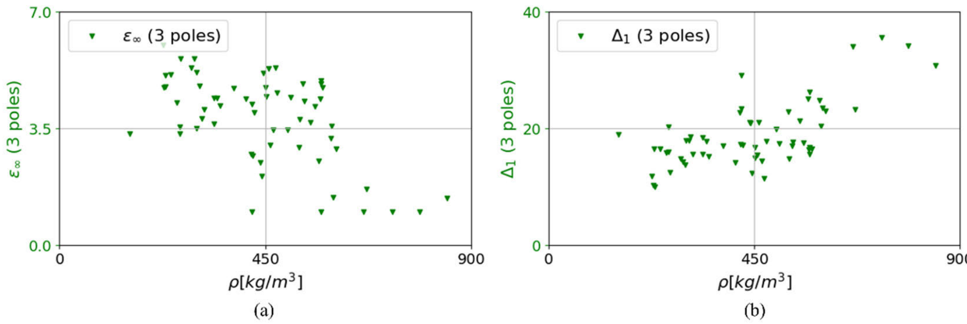

Fig. 5. Three-pole fitting results. (a) Obtained values of ε_∞ for each cube. (b) Obtained values of Δ_1 for each cube.

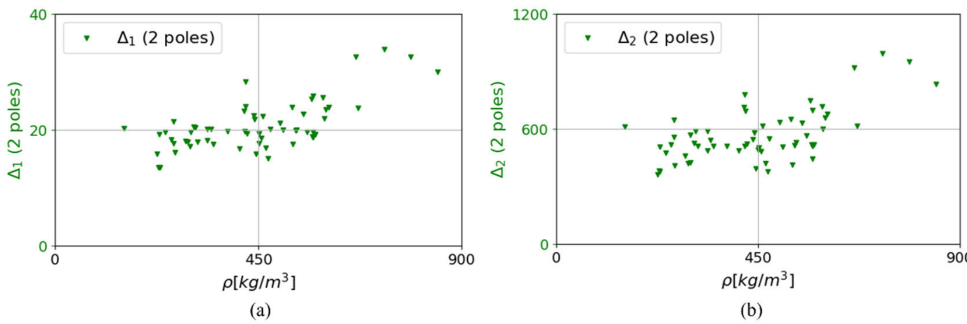

Fig. 6. Two-pole fitting results. (a) Obtained values of Δ_1 for each cube. (b) Obtained values of Δ_2 for each cube.

TABLE III
STARTING BOUNDARIES USED FOR THE TWO-POLE COLE–COLE MODEL FITTING AND THE FIXED PARAMETER VALUES FOR THE SECOND FITTING

Boundary type	ε_∞	Δ_1	$\tau_1\,[ps]$	Δ_2	$\tau_2\,[ns]$	σ_s
Lower	2	3	6.556	10	29.3	0.001
Upper	4	35	231.1	1000	140	0.1
Fixed values	2	/	6.6	/	29.3	0.1

2) Two-Pole Cole–Cole Model Fitting: For the two-pole Cole–Cole model, for the first fitting step, the values of α_1 and α_2 were again fixed to the values given in Table I. The remaining parameters ε_∞, Δ_1, τ_1, Δ_2, τ_2, and σ_s were fitted within the limits given in the first two rows of Table III. The initial boundaries were chosen based on the observation of the existing parameters (see Table I) as in case of the three-pole fitting. Still, these values were unable to produce accurate fitting in the higher frequency range for the two-pole Cole–Cole fitting. Therefore, in this case, the fitting boundaries were chosen based on trial and error. As in the three-pole fitting case, parameters ε_∞, Δ_2, τ_1, τ_2, and σ_s converged to the same value for the majority of the cubes. The second fitting step was performed twice, with different parameters being fixed and fitted. Parameters τ_1, τ_2, and σ_s were fixed for both attempts; in the first attempt, Δ_2 was also fixed, while the fitted parameters were ε_∞ and Δ_1; in the second attempt, ε_∞ was fixed instead while the fitted parameters were Δ_1 and Δ_2 (see Fig. 6). Finally, the latter option was considered more appropriate due to the lower fitting error. The final fixed parameter values are given in the third row of Table III.

The fitting error of the two-pole fitting for the real part of complex permittivity is slightly larger than in case of the three-pole fitting (up to 4%). For the imaginary part of permittivity, the two-pole fitting outperforms the three-pole fitting with error below 3.5% for all samples. Thus, even if the two-pole fitting returns an error value double than the three-pole fitting for the real part, overall, the fitting error achieved by the two-pole Cole–Cole model is below 5%.

3) Density Correlation With Dielectric Properties: Fig. 7 shows the real part of complex permittivity at 2.45 GHz as well as Δ_1 and Δ_2 values obtained from two-pole fitting against density. It is noticeable that permittivity and conductivity increase with density. The same trend is observed at all investigated frequencies. The Pearson correlation coefficient was calculated [29]; this coefficient indicates how strongly two variables are connected. If it is equal to 1 or -1, it signifies that there is a perfect positive or negative linear correlation, respectively. In this case, it is equal to 0.67, meaning that there is a positive correlation between permittivity and density.

As seen in Fig. 7, when permittivity (at 2.45 GHz) and Δ_1 and Δ_2 values obtained from two-pole fitting are plotted against density, the values overlap. Accordingly, it can be inferred that the correlation between density and dielectric properties is embedded in Δ_1 and Δ_2, i.e., in the gap in permittivity associated to the relaxation mechanisms. It is worth noting here that, given the associated time constants of the two poles, the involved relaxation mechanisms are γ dispersion, i.e., water polarization [τ_1 (ps)], and either β or δ dispersion, i.e., interfacial polarization or bound-water polarization [τ_2 (ns)] [30].

Fig. 7(a) and (b) shows that the parameter values increase with density, but this increase is not steep for cubes with density below 575 kg/m^3.

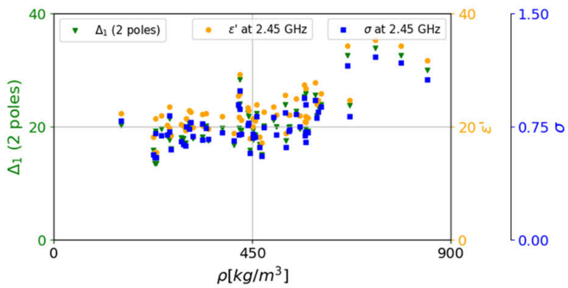

(a)

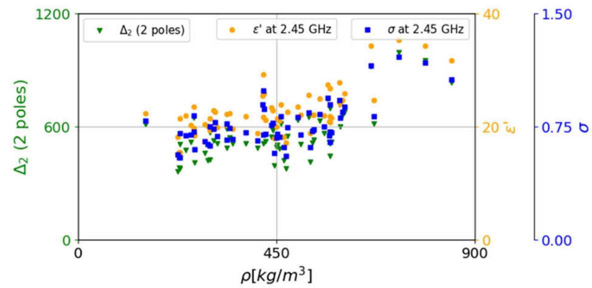

(b)

Fig. 7. (a) Obtained values of Δ_1 with ε' and σ at 2.45 GHz for each cube. (b) Obtained values of Δ_2 with ε' and σ' at 2.45 GHz for each cube.

TABLE IV
Δ_1 AND Δ_2 AVERAGE VALUES FOR BOTH DENSITY RANGES

	Δ_1 $\rho < 575$ kg/m^3	Δ_1 $\rho > 575$ kg/m^3	Δ_2 $\rho < 575$ kg/m^3	Δ_2 $\rho > 575$ kg/m^3
Median	19.54	25.59	514.08	715.76
Mean	19.50	27.48	527.77	779.00
Q_1	17.69	23.58	474.75	635.14
Q_3	20.44	32.54	584.96	933.78
IQR	2.75	8.96	110.21	298.64
St.dev.	2.06	6.72	82.66	223.98

Therefore, the average values of Δ_1 and Δ_2 were calculated for the density ranges 153–575 and 576–847 kg/m^3. The resulting values and uncertainty of the two parameters are listed in Table IV.

IV. Discussion

In this article, the density and dielectric properties in the frequency range 500 MHz–8 GHz of 79 cubic-shaped samples of ex vivo ovine lung tissue were measured. With five out of six lungs inflated prior to sampling, a wide range of lung inflation levels, densities, and dielectric properties was covered, beyond the currently available references [13]. Measurements show that there is no one nominal density of inflated lung rather a range of densities. Additionally, dielectric properties positively correlate with level of inflation. However, measured densities and dielectric properties of the cubic samples were very diverse, as it is expected for a very heterogeneous tissue. Measured data are within the range of data published in the literature. Nonetheless, it should be noted that the experimental and measurement conditions for lung samples in [5] are underdefined.

Different mixture equations were considered to represent the lung dielectric properties as a function of the amount of air present in each cube (results not reported). Mixture theories calculate the effective permittivity of a heterogeneous mixture based on the permittivity of the "main" material (solvent in case of liquids) and the permittivity of the inclusion. In this case, the permittivity of the fully deflated lung from literature was considered as the "main" material [5], and the reference density for the fully deflated lung was used to determine inclusion (i.e., air) content [13]. Several formulas for calculating the dielectric properties of tissue were suggested by Gabriel [30] and therefore applied on lung measurements in this experiment: Foster and Schepps [31], Böttcher [32], Bruggeman [33], Looyenga [34], and Nelson [35] formula. Still, none of these formulas yielded effective permittivity, which deviated less than 10% from the measured data.

An extensive analysis was conducted adopting different pole Cole–Cole models and a two-step fitting procedure. Measured dielectric properties of all samples were successfully fitted to three- and two-pole Cole–Cole models. Given the lower residual error, the two-pole Cole–Cole model was considered the most successful for the intended modeling in the considered frequency range. Additionally, considering that the fitted values of the two-pole Cole–Cole model parameters Δ_1 and Δ_2 exhibited the same increasing trend with density as the measured dielectric properties, it was concluded that the information about density is embedded in these two parameters. To gain a bit of insight into the physics behind the Cole–Cole model, it is worth mentioning that air shows no dispersion behavior; accordingly, the dispersion behavior is linked to the lung tissue only. Since Δ_1 and Δ_2 represent the magnitude of dispersion, their increase with density is expected. In the case of lower density, the air cavities within the tissue are filled with air, and in return, the volume occupied by the water/blood-dominated constituents decreases. In the case of higher density, less air is present, and the sensed volume is dominated by the water/blood constituents. Parameters τ_i represent relaxation times, linked to the two relaxation mechanisms present in the investigated frequency band, γ and β, which remain unchanged with the change in air content across frequency, indicating no change in cellular structure of the tissue (no water loss or chemical reactions on the cellular level). Similarly, ε_∞ represents the permittivity at very high frequencies, where the different dispersion mechanisms are not present anymore. Accordingly, its limit to the lowest value is expectable. Since the increase of these parameters below ~575 kg/m^3 is not so steep, an average value of the two fitted parameters could be given for the lower density range.

On the other hand, this indicates the existence of air content threshold below which the properties begin to change drastically with the change in density. In order to investigate this correlation further, a study on higher density samples would be needed.

V. Conclusion

Lung dielectric properties have been poorly characterized to date, and it is paramount to investigate them to improve microwave-based clinical solutions for treating lung cancer. Lung tissue is very heterogenic and characterized by its inflation levels that in turn influence the tissue density. Therefore, the density and dielectric properties in the 0.5–8 GHz range of 79 samples extracted from ex vivo ovine lung tissue were measured and fitted to two-pole Cole–Cole relaxation models. Density data were used to estimate the air content of the tissue with respect to the reference values reported for inflated and deflated lungs from the literature. Among the relaxation model parameters fitted, Δ_1 and Δ_2, the representatives of the γ and β dispersion magnitudes, respectively, showed correlation to the density of the samples. The parameters' values increase with increasing density, i.e., with decreasing air content.

Acknowledgment

This work has been developed within the framework of COST Action MyWAVE (CA17115).

References

[1] P. M. Meaney, K. D. Paulsen, A. Hartov, and R. K. Crane, "Microwave imaging for tissue assessment: Initial evaluation in multitarget tissue-equivalent phantoms," *IEEE Trans. Biomed. Eng.*, vol. 43, no. 9, pp. 878–890, Sep. 1996.

[2] M. Wang, L. Crocco, and M. Cavagnaro, "On the design of a microwave imaging system to monitor thermal ablation of liver tumors," *IEEE J. Electromagn., RF Microw. Med. Biol.*, vol. 5, no. 3, pp. 231–237, Sep. 2021.

[3] O. J. Babarinde, M. F. Jamlos, P. J. Soh, D. M. M.-P. Schreurs, and A. Beyer, "Microwave imaging technique for lung tumour detection," in *Proc. German Microw. Conf. (GeMiC)*, Bochum, Germany, Mar. 2016, pp. 100–103.

[4] V. Lopresto, R. Pinto, G. A. Lovisolo, and M. Cavagnaro, "Changes in the dielectric properties of ex vivo bovine liver during microwave thermal ablation at 2.45 GHz," *Phys. Med. Biol.*, vol. 57, no. 8, pp. 2309–2327, Apr. 2012.

[5] C. Gabriel and S. Gabriel. (1997). *Compilation of the Dielectric Properties of Body Tissues at RF and Microwave Frequencies (CNR Database)*. Accessed: Apr. 10, 2022. [Online]. Available: http://niremf.ifac.cnr.it/docs/DIELECTRIC/AppendixC.html

[6] A. Fornes-Leal et al., "Dielectric characterization of in vivo abdominal and thoracic tissues in the 0.5–26.5 GHz frequency band for wireless body area networks," *IEEE Access*, vol. 7, pp. 31854–31864, 2019.

[7] L. Abdilla, C. Sammut, and L. Z. Mangion, "Dielectric properties of muscle and liver from 500 MHz-40 GHz," *Electromagn. Biol. Med.*, vol. 32, no. 2, pp. 244–252, Jun. 2013.

[8] D. A. Pollacco, L. Farina, P. S. Wismayer, L. Farrugia, and C. V. Sammut, "Characterization of the dielectric properties of biological tissues and their correlation to tissue hydration," *IEEE Trans. Dielectr. Electr. Insul.*, vol. 25, no. 6, pp. 2191–2197, Dec. 2018.

[9] M. Lazebnik et al., "A large-scale study of the ultrawideband microwave dielectric properties of normal, benign and malignant breast tissues obtained from cancer surgeries," *Phys. Med. Biol.*, vol. 52, no. 20, pp. 6093–6115, Oct. 2007.

[10] World Health Organization. (Feb. 3, 2022). *World Health Organization Website*. Accessed: Apr. 10, 2022. [Online]. Available: https://www.who.int/news-room/fact-sheets/detail/cancer

[11] M. A. Pritchett, K. Bhadra, and J. S. Mattingley, "Electromagnetic navigation bronchoscopy with tomosynthesis-based visualization and positional correction: Three-dimensional accuracy as confirmed by cone-beam computed tomography," *J. Bronchol. Intervent. Pulmonol.*, vol. 28, no. 1, pp. 10–20, Jan. 2021.

[12] L. Farina, G. Ruvio, and M. O'Halloran, "Lung tumor mimicking models for usability validation of transbronchial microwave thermal ablation procedures," in *Proc. IEEE Int. Conf. Microw., Antennas, Commun. Electron. Syst. (COMCAS)*, Tel Aviv, Israel, Nov. 2021, pp. 135–139.

[13] P. Hasgall et al. (Feb. 22, 2022). *IT'IS Database for Thermal and Electromagnetic Parameters of Biological Tissues, Version 4.1*. Accessed: Apr. 10, 2022. [Online]. Available: https://itis.swiss/database

[14] F. A. Duck, "Mechanical properties of tissue," in *Physical Properties of Tissues*. Amsterdam, The Netherlands: Elsevier, 1990, pp. 137–165.

[15] J. Bonello, M. A. Elahi, E. Porter, M. O'Hollaran, L. Farrugia, and C. V. Sammut, "An investigation of the variation of dielectric properties of ovine lung tissue with temperature," *Biomed. Phys. Eng. Exp.*, vol. 5, no. 4, Jun. 2019, Art. no. 045024.

[16] J. Sebek, R. Bortel, and P. Prakash, "Broadband lung dielectric properties over the ablative temperature range: Experimental measurements and parametric models," *Med. Phys.*, vol. 46, no. 10, pp. 4291–4303, Oct. 2019.

[17] P. Nopp, E. Rapp, H. Pfutzner, H. Nakesch, and C. Rusham, "Dielectric properties of lung tissue as a function of air content," *Phys. Med. Biol.*, vol. 38, no. 6, pp. 699–716, Jun. 1993.

[18] S. Etoz and C. L. Brace, "Development of water content dependent tissue dielectric property models," *IEEE J. Electromagn., RF Microw. Med. Biol.*, vol. 3, no. 2, pp. 105–110, Jun. 2019.

[19] K. S. Cole and R. H. Cole, "Dispersion and absorption in dielectrics I. Alternating current characteristics," *J. Chem. Phys.*, vol. 9, no. 4, pp. 341–351, Apr. 1941.

[20] E. C. Burdette, F. L. Cain, and J. Seals, "In vivo probe measurement technique for determining dielectric properties at VHF through microwave frequencies," *IEEE Trans. Microw. Theory Techn.*, vol. MTT-28, no. 4, pp. 414–427, Apr. 1980.

[21] H. U. Rothen, P. Neumann, J. E. Berglund, J. Valtysson, A. Magnusson, and G. Hedenstierna, "Dynamics of re-expansion of atelectasis during general anaesthesia," *Brit. J. Anaesthesia*, vol. 82, no. 4, pp. 551–556, Apr. 1999.

[22] N. P. Silva, A. Bottiglieri, R. C. Conceição, M. O'Halloran, and L. Farina, "Characterisation of ex vivo liver thermal properties for electromagnetic-based hyperthermic therapies," *Sensors*, vol. 20, no. 10, p. 3004, May 2020.

[23] B. N. Taylor and C. E. Kuyatt, "Guidelines for evaluating and expressing the uncertainty of NIST measurement results," NIST, Gaithersburg, MD, USA, Tech. Note 1297, 1994.

[24] A. La Gioia et al., "Open-ended coaxial probe technique for dielectric measurement of biological tissues: Challenges and common practices," *Diagnostics*, vol. 8, no. 2, p. 40, Jun. 2018.

[25] A. Peyman, C. Gabriel, and E. H. Grant, "Complex permittivity of sodium chloride solutions at microwave frequencies," *Bioelectromagnetics*, vol. 28, no. 4, pp. 264–274, May 2007.

[26] C. Gabriel and A. Peyman, "Dielectric measurement: Error analysis and assessment of uncertainty," *Phys. Med. Biol.*, vol. 51, no. 23, pp. 6033–6046, Dec. 2006.

[27] S. Salahuddin, E. Porter, F. Krewer, and M. O'Halloran, "Optimised analytical models of the dielectric properties of biological tissue," *Med. Eng. Phys.*, vol. 43, pp. 103–111, May 2017.

[28] Keysight Technologies. (Dec. 2017). *Keysight 85070E Dielectric Probe Kit 200 MHz to 50 GHz—Technical Overview*. Accessed: Apr. 29, 2022. [Online]. Available: https://www.keysight.com/us/en/assets/7018-01196/technical-overviews/5989-0222.pdf

[29] W. Kirch, Ed., "Pearson's correlation coefficient," in *Encyclopedia of Public Health*. Dordrecht, The Netherlands: Springer, 2008, pp. 1090–1091.

[30] G. Gabriel, "Dielectric properties of biological materials," in *Bioengineering and Biophysical Aspects of Electromagnetic Fields*, 3rd ed. New York, NY, USA: Taylor & Francis, 2006.

[31] K. R. Foster and J. L. Schepps, "Dielectric properties of tumor and normal tissues at radio through microwave frequencies," *J. Microw. Power*, vol. 16, no. 2, pp. 107–119, Jan. 1981.

[32] C. J. F. Böttcher, *Theory of Electric Polarization*. Amsterdam, The Netherlands: Elsevier, 1978.

[33] D. A. G. Bruggeman, "Berechnung verschiedener physikalischer Konstanten von heterogenen substanzen. I. Dielektrizitätskonstanten und leitfähigkeiten der mischkörper aus isotropen substanzen," *Ann. Phys.*, vol. 416, no. 8, pp. 665–679, 1935.

[34] H. Looyenga, "Dielectric constants of heterogeneous mixtures," *Physica*, vol. 31, no. 3, pp. 401–406, Mar. 1965.

[35] S. O. Nelson, "Density dependence of the dielectric properties of wheat and whole-wheat flour," *J. Microw. Power*, vol. 19, no. 1, pp. 55–64, Jan. 1984.

Open Access funding provided by 'Università degli Studi di Roma "La Sapienza"' within the CRUI CARE Agreement